Indian Journal of Pure & Applied Physics
Vol. 62, August 2024, pp. 670-681
DOI: 10.56042/ijpap.v62i8.9202

Exploring the Synergistic Impact of Radiation and Heat Generation on Magnetohydrodynamic Nanofluid Flow through a Variable Darcy-Forchheimer Porous Medium

Ram Prakash Sharma[a,*] & Debasish Gorai[b]

[a]Department of Mechanical Engineering, NIT Arunachal Pradesh 791 113, India
[b]Department of Basic and Applied Science, NIT Arunachal Pradesh 791 113, India

Received 1 March 2024; accepted 20 May 2024

Flow through porous media has wide applications in industry. Many researchers investigated fluid flow over constant porous media, but porous media is not always constant. Thus, the main motive of the current investigation is to know the MHD flow of nanofluid through a variable Darcy-Forchheimer porous intermediate in a rotating disk. Additionally, heat generation and thermal radiation are used in the governing model. Buongiorno model of nanofluid are used. After the transformation of governing equations into ODE problems by some suitable similarity variables, we solve numerically through the R-K 4th-order method with the help of shooting approximation. Engineering-interested coefficients are calculated in this article. The result shows that variable permeability and variable porosity have reverse behaviour for velocity profile, temperature profile as well as engineering coefficients. Overall, this article will help researchers in science and engineering to understand the flow behaviour through variable Darcy-Forchheimer magnetic porous medium.

Keywords: Thermal radiation; Heat source/sink; Darcy-Forchheimer medium; Variable porosity; Permeability

1 Introduction

Fluid flow and heat transport via permeable media is one of the most significant topics of modern engineering research. The term "porous media" refers to a solid medium with pores. Because porous media have so many different applications, flow over them is of great interest to mathematicians and engineers. Significant applications for permeable media include blood circulation within the body, water purification, and oil sanitization. Darcy-Forchheimer rule, which is an extension of Darcy rule, governs the flow model of filling porous material. The fluid movement through porous media was started by Darcy. Then Forchheimer expanded Darcy's equation by adding a new term. He modified the governing momentum equation by adding the square term of the velocity component. Mohanty *et al.*[1] have analyzed the heat transport investigation of fluid flow over a porous extending sheet. Using Kummer's function, Jena *et al.*[2] studied the magnetic field effect on Jeffrey fluid flow in a porous medium. Saif *et al.*[3] have addressed the convective boundary conditions on fluid flow with Darcy-Forchheimer porosity. Ullah *et al.*[4] have examined the 3D Darcy-Forchheimer movement on a spinning disk with a heat sink and slip condition. Rasool *et al.*[5] have examined the fluid movementover a nonlinear stretch sheet in a permeable Darcy-Forchheimer medium. The porosity factor plays an important role in engineering coefficients in their examination. Saif *et al.*[6] conveyed that the fluid flow over the Darcy medium with magnetic behaviour. They take the properties of thermal conductivity of fluid and medium porosity as variable quantity. Hayat *et al.*[7] addressed the unsteady flow via variable permeability and porosity of the Darcy-Forchheimer medium. Saeed *et al.*[8] calculated the hybrid nanofluid flow over the Darcy-Forchheimer medium with a magnetic field. Al_2O_3 and Cu were taken as nanoparticles with water as the main fluid. Shafiq *et al.*[9] premeditated the consequence of convective boundary and thermal slip conditions on 3D nanofluid flow in a permeable medium. Abbas *et al.*[10] have studied the Darcy-Forchheimer nanofluid flow in the presence of radiation, Joule heating, and dissipation. Jena *et al.*[11] scrutinized heat transfer analysis through aabsorbent medium, taking into account heat source/sink effects. Hayat *et al.*[12] inspected the impressions of slip and viscous dissipationon nanoliquid flow in curved sheets. Khan and Alzahrani[13] have addressed the

*Corresponding author:
(E-mail: ramprakash0808@gmail.com)

effect of heat source and slip conditions on viscous nano-liquid flow over a stretched porous surface. Pattnaik *et al*.[14] presented the EMHD flow through a porous medium and discussed the engineering coefficients graphically. Haider *et al*.[15] studied the 3D hybrid nanofluid flow with variable characteristics of porous medium. Pattnaik *et al*.[16] examined the homogeneous and heterogenous reaction effects on nanofluid flow over a Darcy-Forchheimer porous medium and they found that Schimdt number and curvature parameter play important roles in mass transfer rate. Sharma *et al*.[17] investigated numerically the thermal radiation impact on a hybrid nanofluid over a Darcy-Forchheimer porous Riga surface. They observed that the Darcy and Forchheimer numbers reduce the Nusselt number. The bearing of the magnetic flux of squeezing flow in Darcy leaky medium was analyzed by Farooq *et al*.[18].

In nature, there are so manyfields which are electrically conducted, and fluid flow through these magnetohydrodynamics is studied. MHD is heavily involved in processes such as the earth's magnetic field, fusion, solar wind, fission reactor cooling, tumor therapy, and X-ray radiation, among others. Thumma & Mishra[19] discussed the consequence of viscous degeneracy and Joule heat on Jeffrey nanofluid flow under multiple slip criteria. Selimefendigil & Oztop[20,26] have reported the importance of a electric field on three-dimensional flow inside the cavity. Pattnaik *et al*.[21] studied the flow of micropolar fluid in the existence of a binary reaction applying the R-K method.Utilizing the 4^{th}-order Runge-Kutta method, Mohanty *et al*.[22] discussed the MHD movement of nanofluid over an extending surface with a thermal radiation effect. Nayak *et al*.[23] presented the radiative nanofluid flow on an elongating sheet with a in constant magnetic field. Jena *et al*.[24] studied the unsteady scenario of nanofluid flow via a permeable medium with an inclined magnetic field influence. In the mathematical formulation, thermal radiation is represented by the Cogley model. Pattnaik *et al*.[25] numerically explored the binary reaction effect on the MHD motion of nanoliquid through an exponential widening sheet. The effect of convective edge conditions on the MHD flow of Williamson nanofluid has been addressed by Srinivasulu & Goud [27]. Parida *et al*.[28] inspected the magnetohydrodynamic movement of dust particles in the presence of radiation. In place of the base fluid, they take water and kerosene and solve them using the bvp5c code in MATLAB. Manna *et al*.[29] calculated the hybrid nanofluid flow on a porous medium, taking the convective heat transformation phenomenon and magnetic field effect. Using the inbuilt program bvp5c in MATLAB, Pattnaik *et al*.[30] studied the heat transfer analysis of nanofluid in the attendance of radiation. Porous medium flow of nanoliquid through an electrically conducting magnetic field discovered by Hassan *et al*.[31]. Mondal *et al*.[32] discussed the heat transport performance of hybrid nanofluid flow with the consequence of porous medium and magnetic field. The significances of radiation and magnetic effect on Casson nanofluid motion with Marangoni conditions have been travelled by Mahesh *et al*.[33]. Das *et al*.[34] studied the squeezing flow between two disks, taking activation energy and magnetic field. Mishra *et al*.[35-36] investigated the entropy generation of magnetohydrodynamic ternary nanofluid flow using the bvp5c technique in MATLAB and found that the chemical reaction parameter and Brinkman number have opposite impacts on entropy generation. Kumar *et al*.[37] statistically analysed the entropy generation of Jeffrey nanofluid in a magnetic field. They also studied the microorganism flow with melting heat conditions.

Heat generation, thermal radiation and other processes are used to raise the temperature of fluid flow. Many researchers look at heat generation and linear thermal radiation of the three processes of heat transfer, thermal radiation is the most important in mechanical engineering due to transferring heat without a medium. In the other two cases, *i.e*., in conduction and convection, medium is required. Hamid *et al*.[38] numerically elaborated the Williamson nanofluid movement with heat generation and radiation impact through porous channels. The impact of Hall current and radiative heat on unsteady fluid motion has been deliberated by Mahanthesh *et al*.[39]. Armaghani *et al*.[40] elaborated on the impact of a discrete heat on the entropy generation study of nanofluid flow in a L-shaped cavity.Waqas *et al*.[41] pondered the MHD Jeffrey nanoliquid flow in the presence of radiative heat. Shamshuddin *et al*.[42] explored the heat, mass, and microorganism transfer of nanoliquid flow via a revolving disk by using the Adomian decomposition method. Kumer *et al*.[43] explored the heat transfer on the exponentially stretching flow of Casson fluid with the influence of magnetic field and radiation effect. Chu *et al*.[44] have discussed the consequence of variable thermal conductivity on convective Rabinowitsch fluid-taking heat generation and radiative heat flux. Oladimeji

et al.[45] solved the problem of MHD nanofluid flow using the finite difference method. They take Darcy-Forchheimer's law in their problem with external force chemical reactions and heat sources. Sharma *et al.*[46] compared the fluid flow over a linear and nonlinear stretching sheet taking a heat source. Sharma and Mishra examined a numerical study on MHD micropolar fluids with radiation and heat sources[47]. Lim *et al.*[48] elucidated the consequence ofchemical reactions on Carreau fluid flow. Sharma *et al.*[49] investigated the melting heat phenomena in radiative energy transfer of Jeffrey nanofluid flow over a Darcy-Forchheimer porous Riga plate. Mahabaleshwar *et al.*[50] pondered the time-dependent flow of Newtonian liquid in the company of linear thermal radiation. Sharma *et al.*[51-52] studied the optimization of the entropy generation in blood-based nanofluid flow with magnetic field and thermal radiation.

Overall, the Darcy-Forchheimer equation and porous media with magnetic field concepts have widespread applications across industries ranging from energy and environmental engineering to biomedical and geotechnical fields, playing a vital role in understanding and solving real-world engineering challenges. According to the author's knowledge the impact of radiation, magnetic field on flow through variable Darcy-Forchheimer porous medium was not yet studied. We investigate the nanofluid flow over a Darcy-Forchheimer porous media with varying porosity and permeability after getting inspiration from the above-mentioned literature survey. Consequently, the impact of magnetic field, radiative heat flux, and heat generation/absorption are also taken. Fluid flow, heat transfer, and mass transfer are calculated in this article. Therefore, the goal of our research is to track the evolution of mass and heat transmission of radiative MHD flow over a revolving disc in a variable Darcy-Forchheimer porous medium. The behaviour of flow concerning different parameters is shown graphically and in tabular form. Finally, the new findings are marked in the conclusion section.

2 Mathematical formulations

The time-dependent three-dimensional flow of nanofluid stated by a revolving disk is examined here. Medium is taken as Darcy-Forchheimer porous medium with variable characteristics. Unsteady angular velocity is given as $\Omega'(t)=\frac{\Omega}{1-bt}$. Magnetic field is taken through the horizontal axis with uniform strength B_0. Fig. 1 indicates the flow configuration of the current study.

Several assumptions underlie our flow model,

- The flow is considered a time-dependent laminar flow of incompressible fluid.
- Darcy-Forchheimer's model is considered in a porous medium.
- The porosity and permeability of the medium are variables.
- Buoyancy force and viscous dissipation are neglected in our study.

Governing equations in the cylindrical coordinate system are presented as[5,12]

$$\frac{\partial u}{\partial r}+\frac{\partial w}{\partial z}+\frac{u}{r}=0, \qquad ...(1)$$

$$\frac{\partial u}{\partial t}+u\frac{\partial u}{\partial r}+w\frac{\partial u}{\partial z}-\frac{v^2}{r}+\frac{1}{\rho}\frac{\partial p}{\partial r}=\upsilon\left(\frac{\partial^2 u}{\partial z^2}\right)-\frac{\upsilon\varepsilon(z)}{K(z)}u-\frac{C_b\varepsilon^2(z)}{\sqrt{K(z)}}u\sqrt{u^2+v^2}-\frac{\sigma B_0^2 u}{\rho}, \qquad ...(2)$$

$$\frac{\partial v}{\partial t}+u\frac{\partial v}{\partial r}+w\frac{\partial v}{\partial z}+\frac{uv}{r}=\upsilon\left(\frac{\partial^2 v}{\partial z^2}\right)-\frac{\upsilon\varepsilon(z)}{K(z)}v-\frac{C_b\varepsilon^2(z)}{\sqrt{K(z)}}v\sqrt{u^2+v^2}-\frac{\sigma B_0^2 v}{\rho}, \qquad ...(3)$$

$$\frac{\partial T}{\partial t}+u\frac{\partial T}{\partial r}+w\frac{\partial T}{\partial z}=\alpha\left(\frac{\partial^2 T}{\partial z^2}\right)+\frac{(\rho C_p)_p}{(\rho C_p)_f}\left(D_B\left(\frac{\partial T}{\partial z}\frac{\partial C}{\partial z}\right)+\frac{D_T}{T_\infty}\left(\frac{\partial T}{\partial z}\right)^2\right)-\frac{1}{(\rho C_p)}\frac{\partial q_r}{\partial z}+\frac{Q}{(\rho C_p)}(T-T_\infty), \qquad ...(4)$$

$$\frac{\partial C}{\partial t}+u\frac{\partial C}{\partial r}+w\frac{\partial C}{\partial z}=D_B\left(\frac{\partial^2 C}{\partial z^2}\right)+\frac{D_T}{T_\infty}\left(\frac{\partial^2 T}{\partial z^2}\right), \qquad ...(5)$$

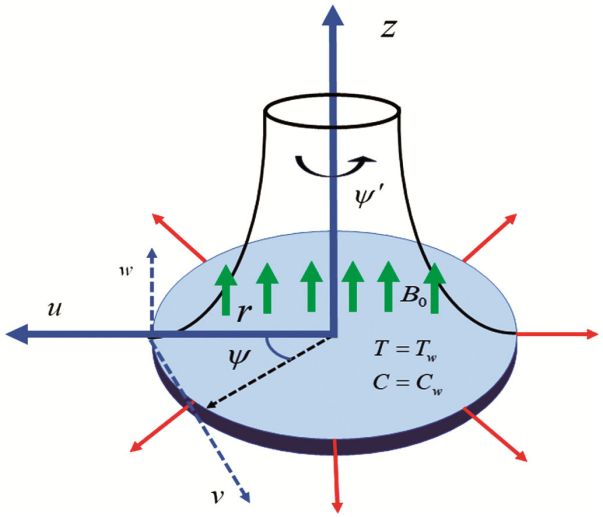

Fig. 1 — Physical configuration of flow

and the above flow equations are allocated with the boundary conditions

$$\left.\begin{aligned} &u=\frac{r\Omega}{1-bt},\ v=\frac{r\Omega}{1-bt},\ w=0,\ T=T_w,\ C=C_w \text{ at } z=0.\\ &u\to 0,\ v\to 0,\ T\to T_\infty,\ C\to C_\infty \text{ as } z\to\infty. \end{aligned}\right\} \quad ...(6)$$

where,

$$K(z)=K_\infty.\left(1+de^{-\eta}\right), \quad ...(7)$$

$$\varepsilon(z)=\varepsilon_\infty.\left(1+d^*e^{-\eta}\right). \quad ...(8)$$

The radiative heat flux in Eq. (4) is simplified by using Rosseland approximation, which can be written as[20],

$$q_r=-\frac{4\sigma^*}{3k^*}\frac{\partial T^4}{\partial z} \quad ...(9)$$

where σ^* be the Stefan Boltzmann coefficient and k^* mean absorption coefficient. Also, expanding T^4 with respect to T_∞ by Taylor series and compacting to a linear function of T we obtain,

$$T^4=4T_\infty^3T-3T_\infty^4 \quad ...(10)$$

Hence,

$$q_r=-\frac{16\sigma^*T_\infty^3}{3k^*}\frac{\partial T}{\partial z} \quad ...(11)$$

After putting the value of q_r from Eq. (11), the simplified form of Eq. (4) is

$$\frac{\partial T}{\partial t}+u\frac{\partial T}{\partial r}+w\frac{\partial T}{\partial z}=\alpha\left(\frac{\partial^2T}{\partial z^2}\right)+\frac{(\rho C)_p}{(\rho C)_f}\left(D_B\left(\frac{\partial T}{\partial z}\frac{\partial C}{\partial z}\right)+\frac{D_T}{T_\infty}\left(\frac{\partial T}{\partial z}\right)^2\right)+\frac{1}{(\rho C_p)}\frac{16\sigma^*T_\infty^3}{3k^*}\frac{\partial^2T}{\partial z^2}+\frac{Q}{(\rho C_p)}(T-T_\infty), \quad ...(12)$$

To transform the modelled equations into dimensionless ordinary form, we take the following similarity variables[5]

$$u=\frac{\Omega r}{1-bt}f'(\eta),\ v=\frac{\Omega r}{1-bt}g(\eta),\ u=-2\sqrt{\frac{\Omega\upsilon}{1-bt}}f(\eta),\ p=\frac{\rho\upsilon\Omega}{1-bt}p(\eta),\ \theta(\eta)=\frac{T-T_\infty}{T_f-T_\infty},\ \phi(\eta)=\frac{C-C_\infty}{C_f-C_\infty},\ \eta=z\sqrt{\frac{\Omega}{\upsilon(1-bt)}}. \quad ...(13)$$

Applying the defined variables in Eqs (1), (2), (3), (5), (6), and (12), we see that Eqn (1) is automatically satisfied, whereas other equations are converted as following form,

$$f'''+2ff''-f'^2-S\left(f'+\frac{\eta}{2}f''\right)+g^2-\beta^*\frac{\left(1+d^*e^{-\eta}\right)^2}{\sqrt{1+de^{-\eta}}}f'\sqrt{f'^2+g^2}-\frac{1}{\delta\,\mathrm{Re}_r}\left(\frac{1+d^*e^{-\eta}}{1+de^{-\eta}}\right)f'-Mf'=0, \quad ...(14)$$

$$g''+2fg'-S\left(\frac{\eta}{2}g'+g\right)-2f'g-\beta^*\frac{\left(1+d^*e^{-\eta}\right)^2}{\sqrt{1+de^{-\eta}}}g\sqrt{f'^2+g^2}-\frac{1}{\delta\,\mathrm{Re}_r}\left(\frac{1+d^*e^{-\eta}}{1+de^{-\eta}}\right)g-Mg=0, \quad ...(15)$$

$$\frac{1}{\mathrm{Pr}}\left(1+\frac{4}{3}Rd\right)\theta''+2f\theta'-\frac{S}{2}\eta\theta'+N_b\theta'\phi'+N_t\theta'^2+\gamma\theta=0, \quad ...(16)$$

$$\phi''+2Scf\phi'-\frac{S}{2}Sc\eta\phi'+\frac{N_t}{N_b}\theta''=0, \quad ...(17)$$

$$\left.\begin{aligned} &f=0,\ f'=1,\ g=1,\ \theta=1,\ \phi=1 \text{ at } \eta=0,\\ &f'\to 0,\ g\to 0,\ \theta\to 0,\ \phi\to 0 \text{ as } \eta\to\infty \end{aligned}\right\} \quad ...(18)$$

Here superscript denotes the differentiation with respect to η and all dimensionless parameters are given below as,

$$S=\frac{b}{\Omega},\ \delta=\frac{K_\infty}{r^2\varepsilon_\infty},\ \mathrm{Re}_r=\frac{U_wr}{\upsilon},\ \beta^*=\frac{C_br\varepsilon_\infty^2}{\sqrt{K_\infty}},\ \mathrm{Pr}=\frac{\upsilon}{\alpha},\ M=\frac{\sigma B_0^2(1-bt)}{\rho\Omega},$$
$$N_b=\frac{\tau D_B}{\upsilon}(C_f-C_\infty),\ N_t=\frac{\tau D_T}{T_\infty\upsilon}(T_f-T_\infty),\ \tau=\frac{(\rho C_p)_p}{(\rho C_p)_f},\ \gamma=\frac{Q(1-bt)}{\Omega(\rho C_p)},$$
$$Rd=\frac{4\sigma^*T_\infty^3}{k^*\kappa},\ Sc=\frac{\upsilon}{D_B}. \quad ...(19)$$

Physical quantities of skin friction coefficient, heat transfer rate, and mass transfer rate have the following expressions:

$$C_f=\frac{\upsilon}{u_w^2}\left(\frac{\partial u}{\partial z}\right)_{z=0},$$
$$C_g=\frac{\upsilon}{v_w^2}\left(\frac{\partial v}{\partial z}\right)_{z=0},$$
$$Nu=-\frac{r}{\kappa(T_f-T_\infty)}\left\{\kappa\left(\frac{\partial T}{\partial z}\right)_{z=0}+\frac{16\sigma^*T_\infty^3}{3k^*}\left(\frac{\partial T}{\partial z}\right)_{z=0}\right\},$$
$$Sh=-\frac{r}{D_B(C_f-C_\infty)}\left(\frac{\partial C}{\partial z}\right)_{z=0}. \quad ...(20)$$

Table 1 — Comparison of present results with previous results of $(\mathrm{Re})^{1/2} Nu_r$ obtained for $M = 0$, $Rd = 0$ and $\gamma = 0$

S	N_b	N_t	Pr	Hayat *et al.*[5]	Oladimeji *et al.*[27]	Present work
0.0	0.2	0.3	0.8	0.23835	0.23321	0.239301

Using similarity variables, dimensionless forms of engineering coefficients are obtained as,

$$\left(\mathrm{Re}_r\right)^{1/2} C_{fr} = f''(0),$$
$$\left(\mathrm{Re}_r\right)^{1/2} C_{gr} = g'(0),$$
$$\left(\mathrm{Re}_r\right)^{-1/2} Nu_r = -\left(1+\frac{4}{3}Rd\right)\theta'(0), \qquad ...(21)$$
$$\left(\mathrm{Re}_r\right)^{-1/2} Sh_r = -\phi'(0).$$

3 Method of solution

As the altered equations are nonlinear, a numerical approach would be preferable. Therefore, Eqs (14-17) are converted into first-order ordinary equations by taking some new variables as follows:

$$\left.\begin{aligned}
&f' = f_1,\\
&f_1' = f_2,\\
&f_{2'} - f_1^2 + 2ff_1 + g^2 - S\left(f_1 + \frac{\eta}{2}f_2\right) - \frac{1}{\delta\,\mathrm{Re}_r}\left(\frac{1+d^*e^{-\eta}}{1+de^{-\eta}}\right)f_1 -\\
&\beta^*\frac{\left(1+d^*e^{-\eta}\right)^2}{\sqrt{1+de^{-\eta}}}\, f_1\sqrt{f_1^2+g^2} - Mf_1 = 0,\\
&g' = g_1,\\
&g_1' - 2f_1g + 2fg_1 - S\left(g + \frac{\eta}{2}g_1\right) - \frac{1}{\delta\,\mathrm{Re}_r}\left(\frac{1+d^*e^{-\eta}}{1+de^{-\eta}}\right)g -\\
&\beta^*\frac{\left(1+d^*e^{-\eta}\right)^2}{\sqrt{1+de^{-\eta}}}\, g\sqrt{f_1^2+g^2} - Mg = 0,\\
&\theta' = \theta_1,\\
&\phi' = \phi_1,\\
&\frac{1}{\mathrm{Pr}}\left(1+\frac{4}{3}Rd\right)\theta_1' + 2f\theta_1 - \frac{S}{2}\eta\theta_1 + N_b\theta_1\phi_1 + N_t\theta_1^2 + \gamma\theta = 0,\\
&\phi_1' + 2Scf\phi_1 - \frac{S}{2}Sc\eta\phi_1 + \frac{N_t}{N_b}\theta_1' = 0,
\end{aligned}\right\} \qquad ...(22)$$

with the boundary conditions,

$$\left.\begin{aligned}
&f = 0,\ f_1 = 1,\ g = 1,\ \theta = 1,\ \phi = 1 \text{ at } \eta = 0,\\
&f_1 \to 0,\ g \to 0,\ \theta \to 0,\ \phi \to 0 \text{ as } \eta \to \infty
\end{aligned}\right\} \qquad ...(23)$$

In Eq. (22), there are nine first-order ordinary differential equations, and Eq. (23) contains nine boundary conditions. Using the shooting method, we convert the above set of equations into an initial value problem and then decode it using the Runge-Kutta 4th-order method of the mathematical software MAPLE. Table 1 is used to validation of our code by comparing the values of $\left(\mathrm{Re}\right)^{1/2} Nu_r$ with Hayat *et al.*[5] & Oladimeji *et al.*[27].

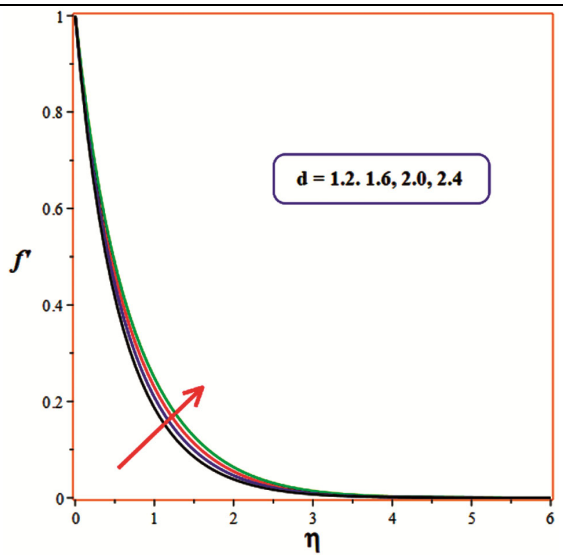

Fig. 2 — Radical velocity profiles $f'(\eta)$ for deviating values of d

4 Results and Discussion

In this section, we discuss the impact of different parameters such as variable permeability (d), variable porosity (d^*), porosity parameter (δ), Brownian motion parameter (N_b), thermophoresis parameter (N_t), Magnetic parameter (M), Schmidt number (Sc) and radiation parameter (Rd) on fluid flow velocity, temperature and mass transfer. Also, the effect of variable parameters on engineering co-efficient skin friction co-efficient, Nusselt number and Sherwood number are depleted by tabular form. Fluid velocity along the radial axis with variable permeability, variable porosity and magnetic parameters are shown in Fig. 2-4. Fig. 2 shows that variable permeability enhances $f'(\eta)$. Fig. 3 plotted to scrutinize the behaviour of $f'(\eta)$ with variable porosity d^*. It is seen that the profile of $f'(\eta)$ is in a downward direction for rising d^*. It ishappening

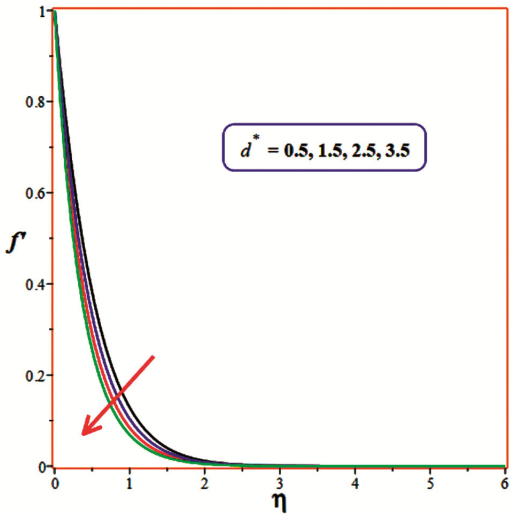

Fig. 3 — Radical velocity profiles $f'(\eta)$ for deviating values of d^*

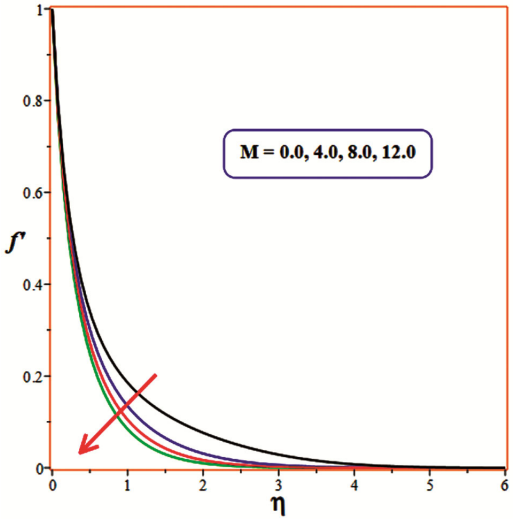

Fig. 4 — Radical velocity profiles $f'(\eta)$ for deviating values of M

because the porosity variable increases, meaning the medium has more void space, and it shrinks more fluid to the medium. From Fig. 2 & 3, we see that $f'(\eta)$ possesses different for d and d^*. The impact of the magnetic field on $f'(\eta)$ is shown in Fig. 4. Since the magnetic field gives a resistance Lorentz force in fluid, thus fluid velocity decreases for M. It is also clear from Fig. 4. Velocity profiles $g(\eta)$ against variable permeability, variable porosity parameter and magnetic parameter are shown in Figs. 5-7. Fig. 5 reflects the rotational velocity $g(\eta)$ against variable permeability, and Fig. 6 shows the effect of the variable porosity parameter on $g(\eta)$. The influence

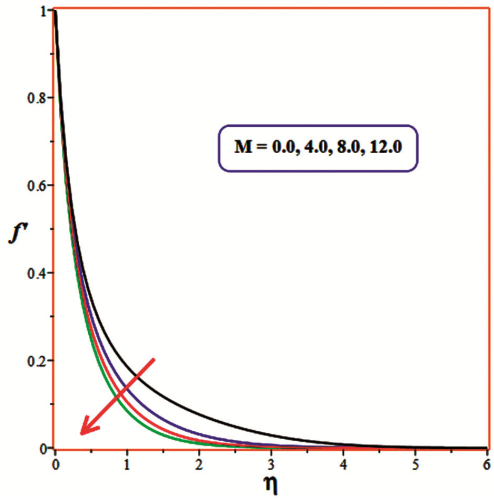

Fig. 5 — Angular velocity profiles $g(\eta)$ for deviating values of d

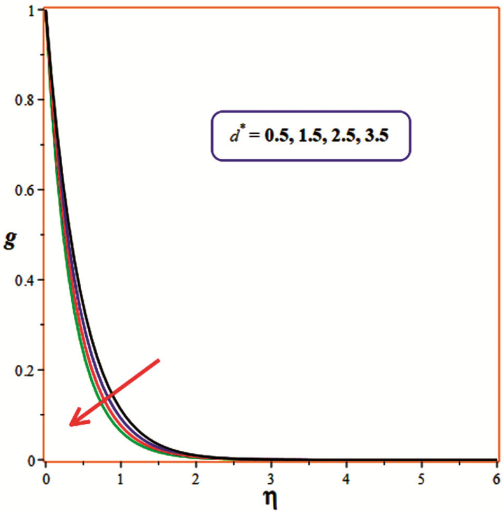

Fig. 6 — Angular velocity profiles $g(\eta)$ for deviating values of d^*

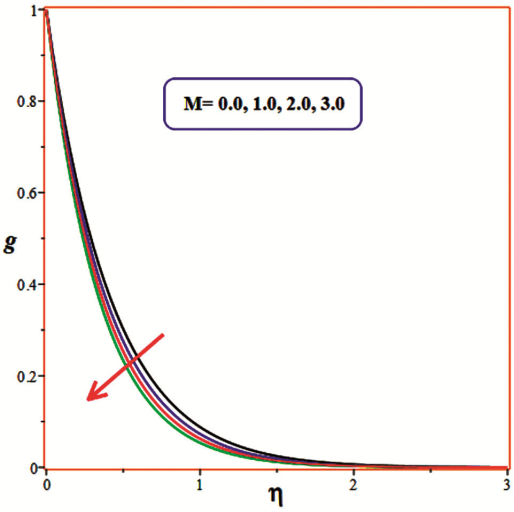

Fig. 7 — Angular velocity profiles $g(\eta)$ for deviating values of M

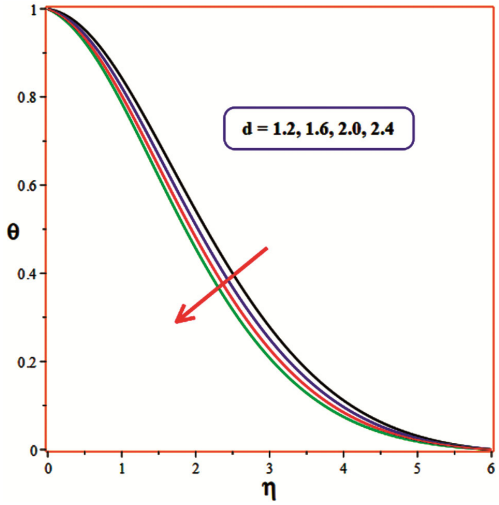

Fig. 8 — Temperature profiles $\theta(\eta)$ for deviating values of d

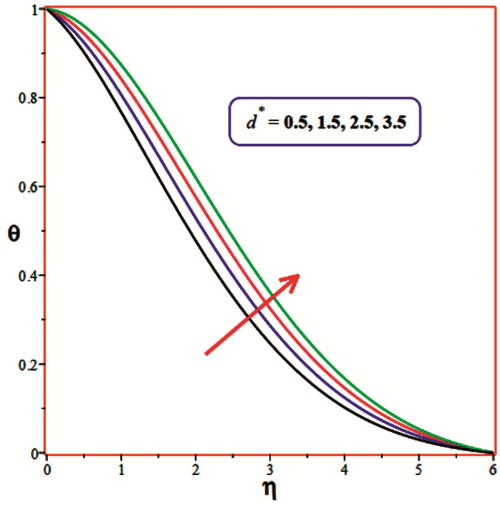

Fig. 9 — Temperature profiles $\theta(\eta)$ for deviating values of d*

of the magnetic field on the velocity component $g(\eta)$ is portrayed in Fig. 7. Here, our result shows that the parameters d and M have the same behavior on $f'(\eta)$ and $g(\eta)$. The consequences of various variables on the temperature field $\theta(\eta)$ are discussed in Fig. 8-13. Fig. 8 presents the behaviour of variable permeability on $\theta(\eta)$. It is seen that $\theta(\eta)$ is inversely proportional to d. Fig. 9 shows that d^* enhance fluid temperature. Fig. 10 witnessed that $\theta(\eta)$ is upward for magnetic field. Since the Lorentz force has a tendency to slow the fluid motion, thus heat of the fluid rises. Fig. 11 elaborated that the radiation parameter and temperature field are proportional to each other. As the thermal radiation

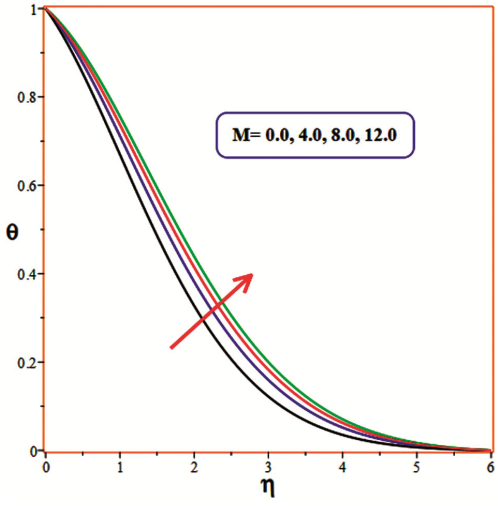

Fig. 10 — Temperature profiles $\theta(\eta)$ for deviating values of M

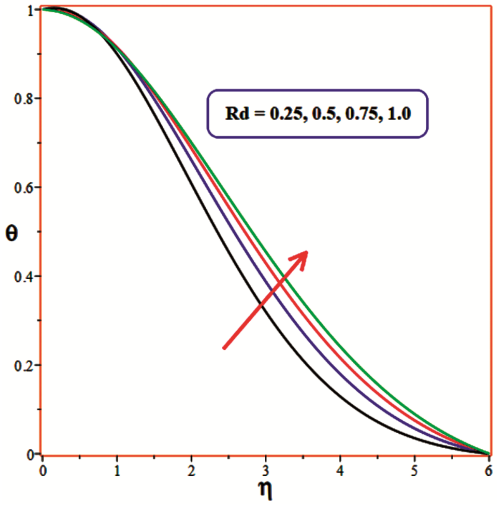

Fig. 11 — Temperature profiles $\theta(\eta)$ for deviating values of Rd

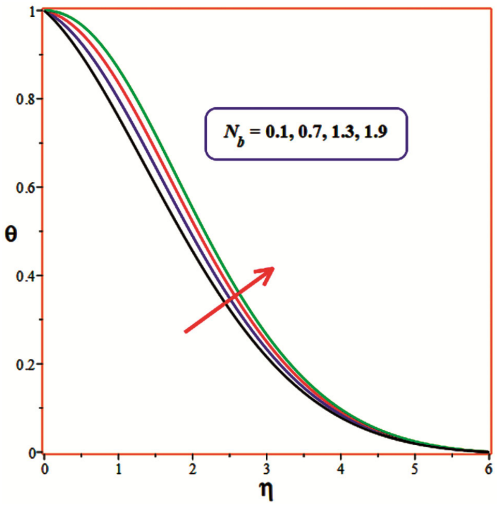

Fig. 12 — Temperature profiles $\theta(\eta)$ for deviating values of N_b

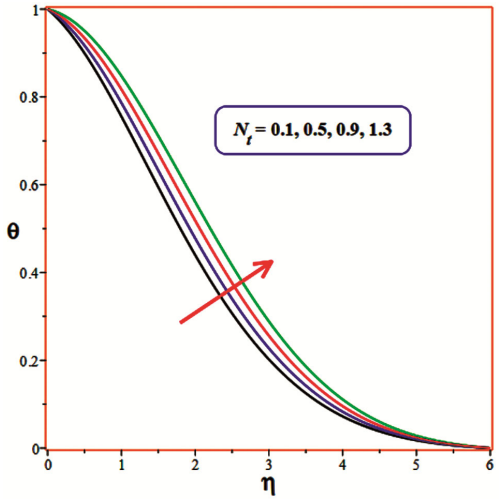

Fig. 13 — Temperature profiles $\theta(\eta)$ for deviating values of N_t

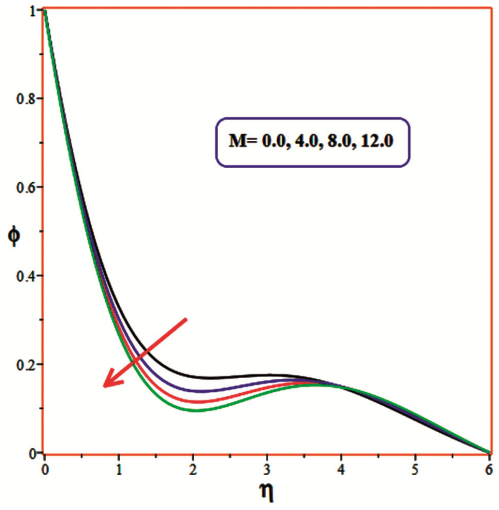

Fig. 14 — Concentration profiles $\phi(\eta)$ for deviating values of M

parameter Rd directly related to heat flux so, Rd increases mean heat flux increases and the temperature also. Impacts of N_b and N_t on $\theta(\eta)$ are deliberated in Fig. 12 & 13. In both cases, temperature strengthens for higher parameter values. Concentration profiles for different parameters are displayed in Fig. 14-17. The magnetic effect on the mass transfer profile is displayed in Fig. 14. Due to the force of resistance, mass transportation is lower for magnetic parameters. Brownian parameter N_b and thermophoresis parameter N_t have antipodal actions sketched in Fig. 15 & 16. Characteristic of Sc on $\phi(\eta)$ is portrayed in Fig. 17. It shows that it Sc lowers the mass transfer $\phi(\eta)$.

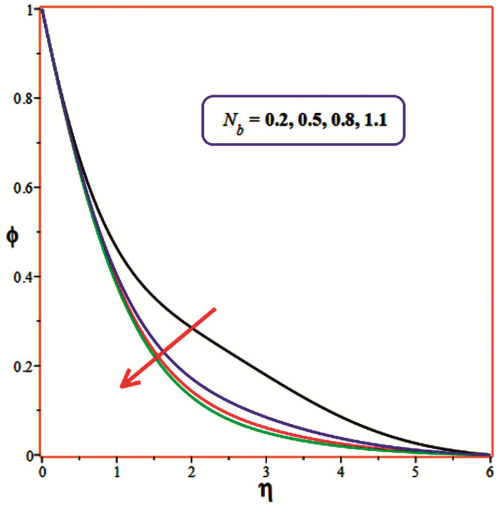

Fig. 15 — Concentration profiles $\phi(\eta)$ for deviating values of N_b

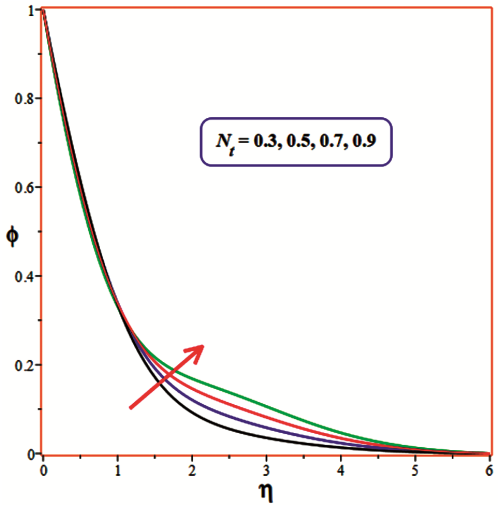

Fig. 16 — Concentration profiles $\phi(\eta)$ for deviating values of N_t

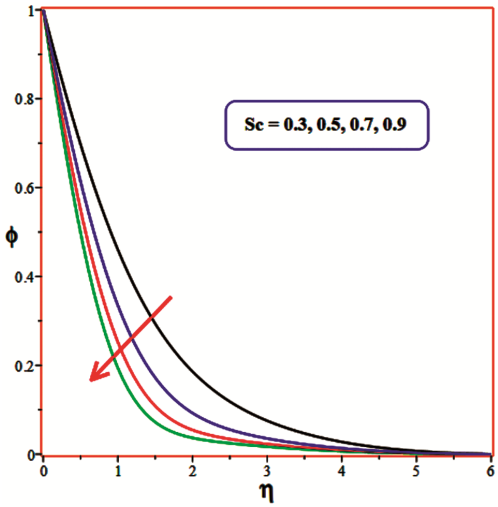

Fig. 17 — Concentration profiles $\phi(\eta)$ for deviating values of Sc

Table 2 — Coefficient of skin friction $-\sqrt{\mathrm{Re}_r}C_{fr}$ and $-\sqrt{\mathrm{Re}_r}C_{gr}$

S	d	d^*	M	$-\sqrt{\mathrm{Re}_r}C_{fr}$	$-\sqrt{\mathrm{Re}_r}C_{gr}$
-0.5	3	1.5	4	2.79171099477888	3.02191599804945
-0.3				2.81766149538301	3.04608430395516
-0.7				2.76560442607880	2.99762161294342
-0.9				2.73934147015788	2.97320115472421
	1			3.26675962029582	3.46702052786698
	2			2.96306784499593	3.18142887967459
	4			2.68035420722458	2.91901682125301
		0.5		2.53136668621260	2.78070695475955
		1		2.66059070212887	2.90003409972463
		2		2.92453223577812	3.14610348694756
			2	2.41122003907717	2.67441740332818
			3	2.60815372392952	2.85323515006506
			5	2.96423435415026	3.18195004865489

Table 3 — Coefficient of Nusselt number $-\left(\mathrm{Re}_r\right)^{-1/2}Nu_r$

S	d	d^*	M	N_b	N_t	Rd	Sc	$-\left(\mathrm{Re}_r\right)^{-1/2}Nu_r$
-0.5	3	1.5	4	0.3	0.2	0.5	0.9	0.008325260007
-0.3								0.3357128232
-0.7								-0.1917814157
-0.9								-0.3319517502
	1							0.08169473705
	2							0.03695885944
	4							-0.01183679158
		0.5						-0.03292856807
		1						-0.01188011460
		2						0.02771141829
			2					-0.07134036278
			3					-0.02864651096
			5					0.04071613152
				0.1				-0.02125014875
				0.5				0.03528034332
				0.7				0.05974312816
					0.1			-0.009609242204
					0.3			0.02630240696
					0.4			0.04435030893
						0.4		0.01025627109
						0.6		0.002893507679
						0.7		-0.005435341144
							1.1	0.005857046735
							1.3	0.003606824482
							1.5	0.001602560632

The engineer's requirement coefficients are shown in three tables. Local friction coefficients C_{fr} and C_{gr} for different parameters are discussed in Table 2. The magnitude of skin friction coefficients d^* and M is enhanced, while the action of s and d is antipode. Local Nusselt number decreases for the magnetic parameter, Brownian motion parameter and thermophoresis parameter, which are shown in Table 3. Table 4 bestowed the computed values of the local mass transfer rate for different parameters. Sherwood's number is rising downward for enhancing the parameters d^*, S, M, N_b and Rd.

Table 4 — Coefficient of Sherwood number $\left(\mathrm{Re}_r\right)^{-1/2} Sh_r$

S	d	d^*	M	N_b	N_t	Rd	Sc	$\left(\mathrm{Re}_r\right)^{-1/2} Sh_r$
-0.5	3	1.5	4	0.3	0.2	0.5	0.9	0.796058880679860
-0.3								0.854227634508756
-0.7								0.790729653644432
-0.9								0.7804079152621082
	1							0.791369091597833
	2							0.794203200328126
	4							0.797389279192155
		0.5						0.799294260634373
		1						0.797606297559969
		2						0.794636462180387
			2					0.801166545489611
			3					0.798290246642241
			5					0.794266566781390
				0.1				0.929993289102788
				0.5				0.768717443198213
				0.7				0.756624559611376
					0.1			0.752347172877990
					0.3			0.845723126723281
					0.4			0.901401057539670
						0.4		0.796813179016201
						0.6		0.794521083952342
						0.7		0.792500390993465
							1.1	0.896243603871575
							1.3	0.990572220532957
							1.5	1.07989969251397

5 Conclusion

In this present study, we have considered the nanofluid flow through a Darcy-Forchheimer porous medium where the medium porosity and permeability are variables. The nature of various parameters is shown by tables and graphs. The conclusions of this study are as follows:

- The behavior of d and d^* in fluid velocity and temperature profileshas the opposite action.
- Due to the magnetic field, the temperature of the fluid rises, and the momentum profile decreases due to resistive force.
- Rd hasa common role in the temperature profile. It enhances the temperature of the fluid.
- Augmentation in concentration is seen for N_t but the nature of N_b, Sc and M are contrary.
- Greater d^* and M augment magnitude of skin friction coefficient.
- The magnitude of local heat and mass transfer rate is reduced S and Rd.

Future scopes and limitations

In this study, we investigate the heat and mass transfer of radiative MHD flow in a Darcy-Forchheimer porous medium with constant fluid thermophysical properties. However, fluid thermophysical properties generally depend on temperature and pressure. So, our study can be extended with variable thermophysical properties, nonlinear radiation and also by adding Joule heating and chemical reaction. Fluid flow problems often require simplifying assumptions to make the mathematical equations more tractable. These assumptions may neglect certain real-world complexities, such as the presence of turbulence, compressibility, or heat transfer effects. While these assumptions can greatly simplify the analysis, they may lead to inaccuracies in certain situations.

Nomenclature

(u, v, w)	Velocity component along r, ψ and z axis $\left(\mathrm{m\,s^{-1}}\right)$

$\Omega'(t)$	Time-dependent angular velocity (s^{-1})
Ω	Angular velocity of disk (s^{-1})
T	Temperature of the fluid at any point (K)
$(T_w,\ T_\infty)$	Temperature of the disk and free fluid (K)
C	Concentration of fluid at any point
$(C_w,\ C_\infty)$	Concentration of fluid at disk and free fluid
B	Unsteadiness constant (s^{-1})
p	Pressure of fluid at any point (Pa)
B_0	Magnetic field strength at any point $(NA^{-1}m^{-1})$
$(K_\infty,\ \varepsilon_\infty)$	Permeability and porosity of medium
$(d,\ d^*)$	Permeability and porosity constant
C_b	Forchheimer drag coefficient
q_r	Radiative heat flux $(W.m^{-2})$
Q	Volumetric rate of heat source $(JK^{-1}m^{-3})$
σ^*	Stefan Boltzmann coefficient $(Wm^{-2}K^{-4})$
k^*	Rosseland mean absorption coefficient (m^{-1})
D_B	Brownian motion diffusion $(\mathrm{m}^2\ \mathrm{s}^{-1})$
D_T	Thermophoresis diffusion $(\mathrm{m}^2\ \mathrm{s}^{-1})$
θ	Dimensionless temperature
ϕ	Dimensionless concentration
S	Dimensionless unsteadiness parameter
M	Magnetic number
Pr	Prandtl number
Rd	Dimensionless thermal radiation
δ	Dimensionless porosity parameter
β^*	Local inertial parameter
γ	Dimensionless heat generation parameter
Nb	Dimensionless Brownian motion parameter
Nt	Dimensionless thermophoresis parameter
Sc	Schmidt number
C_{fr}	Local skin friction coefficient
Nu_r	Local Nusselt number
Sh_r	Local Sherwood number
Re_r	Local Reynolds number
μ	Dynamic viscosity of the fluid $(\mathrm{kg\ m^{-1}\ s^{-1}})$
υ	Kinematic coefficient of viscosity $(\mathrm{m^2\ s^{-1}})$
ρ	Density $(\mathrm{kg\ m^{-3}})$
c_p	Specific heat capacity $(JKg^{-1}K^{-1})$
σ	Electrical conductivity $(\mathrm{simens.m^{-1}})$
κ	Thermal conductivity $(\mathrm{Wm^{-1}K^{-1}})$
τ	Ratio of effective heat capacity of nanoparticle and fluid

Declarations

Conflict of interest

The authors declare that there is no conflict of interest.

Data availability

There is no hidden data and all the data available from literature and it is open source.

References

1 Mohanty B, Mishra S R & Pattnayak H B, *Alex Eng J*, 54 (2015) 223.
2 Jena S, Mishra S R & Dash G C, *Int J Appl Comput Math*, 3 (2017) 1225.
3 Saif R S, Hayat T, Ellahi R, Muhammad T & Alsaedi A, *Int J Numer Method H*, 29 (2019) 2.
4 Ullah M Z, Capizzano S S & Baleanu D, *Front Phys*, 7 (2019) 219.
5 Rasool G, Shafiq A, Khalique C M & Zhang T, *Phys Scr*, 94 (2019) 105221.
6 Saif R S, Muhammad T & Sadia H, *Physica A*, 551 (2020) 124067.
7 Hayat T, Haider F, Alsaedi A & Ahmad B, *Int Commun Heat Mass Transf*, 119 (2020) 104904.
8 Saeed A, Tassaddiq A, Khan A, Jawad M, Deebani W, Shah Z & Islam S, *Coating*, 10 (2020) 391.
9 Shafiq A, Rasool G & Khalique C M, *Symmetry*, 12 (2020) 741.
10 Abbas S Z, Khan W A, Kadry S, Khan M I, Waqas M & Khan M I, *Comput Meth Programs Biomed,* 190 (2020) 105363.
11 Jena S, Mishra S R, Pattnaik P K & Sharma R P, *Lat Am Appl Res*, 50 (2020) 283.
12 Hayat T, Qayyum S, Alsaedi A & Ahmad B, *Int Commun Heat Mass Transf*, 111 (2020) 104405.
13 Khan M I & Alzahrani F, *Int J Hydrog Energy*, 46 (2021) 1362.
14 Pattnaik P K, Mohapatra D K & Mishra S R, *Recent Trends in Applied Mathematics: Select Proceedings of AMSE 2019*, (2021) 307.
15 Haider F, Hayat T & Alsaedi A, *Alex Eng J*, 60 (2021) 3047.
16 Pattnaik P K, Mishra S R, Beg O A, Khan U F & Umavathi J C, *Mater Sci Eng B*, 277 (2022) 115589.
17 Sharma B K, Kumar A, Almohsen B & Gamiz U F, *Case Stud Therm Eng*, 51 (2023) 103642.

18 Farooq M, Walie M H, Ahmad S & Hassine S B H, *Int Commun Heat Mass Transf*, 146 (2023) 106945.
19 Thumma T & Mishra S R, *J Nanofluids*, 7 (2018) 516.
20 Selimefendigil F & Oztop H F, *Int Commun Heat Mass Transf*, 95 (2018) 182.
21 Pattnaik P K, Jena S, Dei A & Sahu G, *JP J Heat Mass Transf*, 18 (2019) 207.
22 Mohanty B, Jena S & Pattnaik P K, *Int J Emerg Technol*, 10 (2019) 119.
23 Nayak M K, Shaw S & Chamkha A J, *Arab J Sci Eng*, 44 (2019) 1269.
24 Jena S, Mishra S R & Pattanaik P K, *J Nanofluids*, 9 (2020) 143.
25 Pattnaik P K, Mishra S R, Barik A K & Mishra A K, *Int J Fluid Mech Res*, 47 (2020) 217.
26 Selimefendigil F & Oztop H F, *J Therm Anal Calorim*, 143 (2021) 1485.
27 Srinivasulu T & Goud B S, *Case Stud Therm Eng*, 23 (2021) 100819.
28 Parida S K, Mishra S R, Dash R K, Pattnaik P K, Khan M I, Chu Y M & Shah F, *Int J Chem React Eng*, 19 (2021) 787.
29 Manna N K, Mondal C, Biswas N, Sarkar U K, Oztop H F & Hamdeh N H A, *Phys Fluids*, 33 (2021) 053604.
30 Pattnaik P K, Pattnaik J R, Mishra S R & Nisar K S, *J Therm Anal Calorim*, 147 (2022) 2537.
31 Hassan A, Hussain A, Arshad M, Haider Q, Althobaiti A, Elagan S K, Alqurashi M S & Abdelmohimen M A H, *Ain Shams Eng J*, 13 (2022) 101667.
32 Mondal M K, Biswas N, Mandal D K, Manna N K & Chamkha A J, *Waves Random Complex Media*, (2022). https://doi.org/10.1080/17455030.2022.2066220.
33 Mahesh R, Mahabaleshwar U S, Aly E H & Manca O, *Int Commun Heat Mass Transf*, 141 (2023) 106561.
34 Das K, Sharma R P & Gorai D, *J Nanofluids*, 12 (2023) 388.
35 Mishra N K, Sharma B K, Sharma P, Muhammad T & Perez L M, *Sci Rep*,13 (2023) 14483.
36 Mishra N K, Sharma P, Sharma B K, Almohsen B & Perez L M, *Heliyon*, 10 (2024) e25102.
37 Kumar A, Sharma B K, Bin-Mohsen B & Gamiz U F, *Int J Numer Method H,* 34 (2024) 948.
38 Hamid M, Usman M, Khan Z H, Haq R U & Wang W, *Eur Phys J Plus*, 133 (2018) 527.
39 Mahanthesh B, Shashikumar N S, Gireesha B J & Animasaun I L, *J Comput Des Eng*, 6 (2019) 551.
40 Armaghani T, Rashad A M, Vahidifar O, Mishra S R & Chamkha A J, *Int J Numer Method H*, 29 (2019) 1363.
41 Waqas M, Shehzad S A, Hayat T, Khan M I & Alsaedi A, *J Phys Chem Solids*, 133 (2019) 45.
42 Shamshuddin M D, Mishra S R, Beg O A & Kadir A, *J Cent South Univ*, 26 (2019) 2797.
43 Kumar K A, Sugunamma V & Sandeep N, *J Them Anal Calorim*, 140 (2020) 2377.
44 Chu Y M, Nazeer M, Khan M I, Hussain F, Rafi H, Qayyum S & Abdelmalek Z, *Int Commun Heat Mass Transf*, 120 (2021) 105011.
45 Oladimeji A A, Wale O A, Obalalu A M, Peter A, Adebayo A O & Alao S, *J Adv Res Appl Sci*, 7 (2021) 1.
46 Sharma R P, Gorai D & Das K, *Heat Transf*, 51 (2022) 6365.
47 Sharma R P & Mishra S R, *J Ocean Eng Sci*, 7 (2022) 92.
48 Lim Y J, Shafie S, Isa S M, Rawi N A & Mohamad A Q, *Alex Eng J*, 61 (2022) 4701.
49 Sharma B K, Kumar A, Mishra N K, Albaijan I & Gamiz U F, *Case Stud Therm Eng*, 52 (2023) 103658.
50 Mahabaleshwar U S, Sneha K N, Perez L M & Manca O, *Int Commun Heat Mass Transf*, 145 (2023) 106844.
51 Sharma B K, Sharma P, Mishra N K, Noeiaghdam S & Gamiz U F, *Alex Eng J*, 77 (2023) 127.
52 Sharma B K, Khanduri U, Mishra N K, Albaijan I & Perez L M, *Sci Rep*, 13 (2023) 154441.